Report

Current Biology

# Reversed Procrastination by Focal Disruption of Medial Frontal Cortex

## Highlights

- Voluntary reaction times are slower and more variable than neural noise explains
- Such procrastination is theorized to reflect a neural race selecting each action
- Electrically disrupting medial frontal cortex reverses procrastination
- A cardinal prediction of race models of action in the brain is thereby confirmed

## Authors

Ashwani Jha, Beate Diehl, Catherine Scott, Andrew W. McEvoy, Parashkev Nachev

## Correspondence

p.nachev@ucl.ac.uk

## In Brief

Studying the effects of direct cortical stimulation of the human medial frontal lobe, Jha et al. report reversal of the natural action delay or "procrastination" long predicted by race models of voluntary action as a fundamental feature of decision-making in the human brain.

Jha et al., 2016, Current Biology *26*, 2893–2898
November 7, 2016 
http://dx.doi.org/10.1016/j.cub.2016.08.016

CellPress

Current Biology
Report

# Reversed Procrastination by Focal Disruption of Medial Frontal Cortex

Ashwani Jha,[1,2] Beate Diehl,[1,2] Catherine Scott,[1,2] Andrew W. McEvoy,[1,2] and Parashkev Nachev[1,2,3,*]
[1]Institute of Neurology, UCL, Queen Square, London WC1N 3BG, UK
[2]National Hospital for Neurology and Neurosurgery, Queen Square, London WC1N 3BG, UK
[3]Lead Contact
*Correspondence: p.nachev@ucl.ac.uk
http://dx.doi.org/10.1016/j.cub.2016.08.016

## SUMMARY

**An enduring puzzle in the neuroscience of voluntary action is the origin of the remarkably wide dispersion of the reaction time distribution, an interval far greater than is explained by synaptic or signal transductive noise [1, 2]. That we are able to change our planned actions—a key criterion of volition [3]—so close to the time of their onset implies decision-making must reach deep into the execution of action itself [4–6]. It has been influentially suggested the reaction time distribution therefore reflects deliberate neural procrastination [7], giving alternative response tendencies sufficient time for fair competition in pursuing a decision threshold that determines which one is behaviorally manifest: a race model, where action selection and execution are closely interrelated [8–11]. Although the medial frontal cortex exhibits a sensitivity to reaction time on functional imaging that is consistent with such a mechanism [12–14], direct evidence from disruptive studies has hitherto been lacking. If movement-generating and movement-delaying neural substrates are closely co-localized here, a large-scale lesion will inevitably mask any acceleration, for the movement itself could be disrupted. Circumventing this problem, here we observed focal intracranial electrical disruption of the medial frontal wall in the context of the pre-surgical evaluation of two patients with epilepsy temporarily reversing such hypothesized procrastination. Effector-specific behavioral acceleration, time-locked to the period of electrical disruption, occurred exclusively at a specific locus at the ventral border of the pre-supplementary motor area. A cardinal prediction of race models of voluntary action is thereby substantiated in the human brain.**

## RESULTS AND DISCUSSION

The transient, focal, "virtual" lesioning effected by intracerebral electrical stimulation of cortex for clinical purposes opens a rare but illuminating window into the operations of the human cortex [15, 16]. Though stringently constrained, behaviorally and anatomically, to the actions and neural loci justified by clinical need, in the two patients studied here the clinical requirements of evaluation for possible epilepsy surgery serendipitously overlapped with the present scientific question. Subdural electrode grids were temporarily implanted on the medial surface, among other areas, of the left frontal lobe, with the aim of identifying a presumed epileptic focus whose location anatomical neuroimaging had not disclosed and for mapping motor areas on the medial wall should a resection there be subsequently indicated (see Supplemental Experimental Procedures and Table S1).

Following standard clinical practice, the patients were asked to perform self-paced, repetitive actions—vocally or manually in different blocks—while electrical current was briefly delivered between pairs of neighboring grid electrodes, one pair at a time, for manually controlled durations of a few seconds [17]. Each action consisted of alternating movements at a frequency the patient chose spontaneously but was asked to maintain at a constant value. In the manual task, the movements were single or multiple finger flexions and extensions at the proximal metacarpophalangeal joints; in the vocal task, the movements were repeated single syllable vocalizations such as "la-la-la" (see Movie S1). Patients were also tested at rest and during natural reading. The electrical stimulation parameters—50 Hz biphasic square wave delivering up to 4 mA of current between two adjacent electrodes 5 mm apart—were within the values generally considered disruptive of underlying neural function [16, 18]. Since cortical stimulation may readily trigger seizure activity, clinical practice constrained behavioral testing to no more than one or two blocks per electrode contact and target behavior.

To establish the underlying anatomy, the electrode locations imaged with computed tomography (CT) were co-registered to a pre-implantation volumetric magnetic resonance (MR) volume, correcting for post-operative brain distortion, with independent manual landmark validation of the result. The images were then non-linearly transformed into standard stereotactic anatomical space (Montreal Neurological Institute [MNI]), guided by the MR image. Individual motor anatomical context was provided by fMRI of noun repetition and verb generation: this highlighted the individual location of the medial motor areas. Each electrode contact on the medial wall was thus localized by individual structural anatomy, MNI template coordinates, and functional markers of speech articulation and generation (Figure 2; see Supplemental Experimental Procedures).

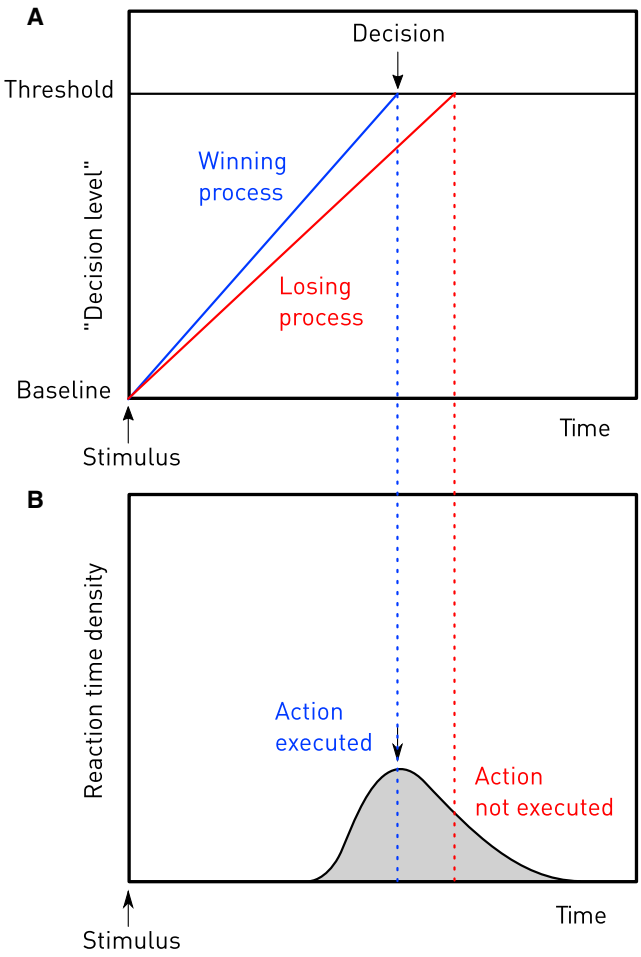


**Figure 1. Decision-Making as a Race**

(A and B) Race models of voluntary action conceive of an ensemble of decision signals embodying a measure of the probability of an action that rise linearly from baseline, each at a given rate, to approach a critical threshold (A). The action executed on any given occasion corresponds to that associated with the signal reaching the threshold first (in blue). Variation in the winner on any one occasion, resulting from variability in the race parameters, generates the characteristic distribution in reaction times (B). Although only two processes are shown here, a multiplicity of processes will compete for the threshold at any one time, reflective of the wide horizon of action possibilities before us. Within the LATER race model employed here, the decision process is conceptualized as a log measure of the probability of the corresponding action. Note that the start of the race is commonly timed by an external stimulus event, but the same principle may apply to any condition relevant to action, including internal physiological states.

The combination of self-pacing and alternating between two isolable actions—finger flexion and extension versus pausing, or vocalization versus glottal arrest—offered as optimal a test of neural procrastination as a coincidence with clinical protocol could be expected to yield. Within the family of race models of action, an ensemble of decision signals embodying a measure of the probability of an action rise linearly from baseline, at a given rate, to approach a critical threshold (Figure 1). The action executed on any given occasion corresponds to the signal reaching the threshold first. Whereas in exogenously driven action, the source of the decision signals is the external environment—visual cues, for example—in endogenously driven, self-paced action, the source might only be internal states reflecting desired goals. And whereas the race outcome may be manifest in the *morphology* of the response—for example, moving a finger left versus right—in self-paced, identically repetitive action, it may be manifest only in the *timing* of the response—for example, low versus high repetition rates. Now, if the race distance is artificially shortened, by either raising the baseline or lowering the threshold, early completion of the race underlying each action will result. In the context of repetitive, self-paced behavior, reversed neural procrastination thus predicts an increase in the overall frequency, whatever the subject's desired pace of alternation.

This is precisely what we observed in each patient, at a location falling within the ventral pre-supplementary motor area on the border between the superior frontal gyrus and the cingulate gyrus, inside 10 mm rostral of the VCA line (Figure 2). Disruptive stimulation here, and only here among all electrode contacts, visibly and audibly increased the frequency of alternation, leaving the morphology of the movement otherwise unchanged (see Movie S1 and Table S2). This inference was formalized by comparing the distributions of inter-movement intervals in blocks immediately before and after stimulation onset, as determined from video telemetry and audio spectral analysis, within a mixed general linear model with stimulation and effector as fixed factors and patient as a random factor (see Supplemental Experimental Procedures). There was a significant main effect of stimulation consisting of an increase in behavioral frequency from a mean of 2.96 Hz (SEM = 0.35) to 3.76 Hz (SEM = 0.34) ($F(1,123)$ = 22.547, $p < 0.001$). The behavioral acceleration was strongly effector specific: in the patient where the electrodes were slightly more rostral, LW, the acceleration was confined to vocalization; in DH, the converse was observed (Figure 2, inset plots, and Table S2). This was reflected in a highly significant three-way interaction of stimulation, patient, and effector ($F(4,123)$ = 9.547, $p < 0.001$), with post hoc t tests confirming in LW a vocal ($p = 0.030$), but not manual, effect ($p = 1.000$), and in DH a manual ($p < 0.001$), but not vocal, effect ($p = 0.098$, all Bonferroni adjusted).

To illuminate the underlying mechanisms, we further modeled the inter-movement intervals as if they were natural reaction times [19, 20], reasonably assuming the timing of each component movement to be relative to endogenous determinants of the self-paced rate of alternation. The duration of each component movement was generally shorter than the inter-movement interval, making such discretization mechanistically plausible. This enabled us to perform a reciprobit analysis where the intervals were transformed to their reciprocals and plotted against their cumulative distribution, on the assumption it is Gaussian after the transformation. The resultant distributions could be adequately modeled by linear functions, demonstrating that a race model, specifically the standard LATER (linear approach to threshold with ergodic rate) model, fits the observed behavior [8, 21] (Figure 3).

Moreover, the change in the underlying function produced by stimulation was exactly as the LATER model would predict if the "decision distance" from baseline to threshold were diminished, i.e., if the race were artificially shortened. In such circumstances, LATER predicts a "swivel" of one function against the other around a fixed intercept at infinity, whereas if the rate of rise of

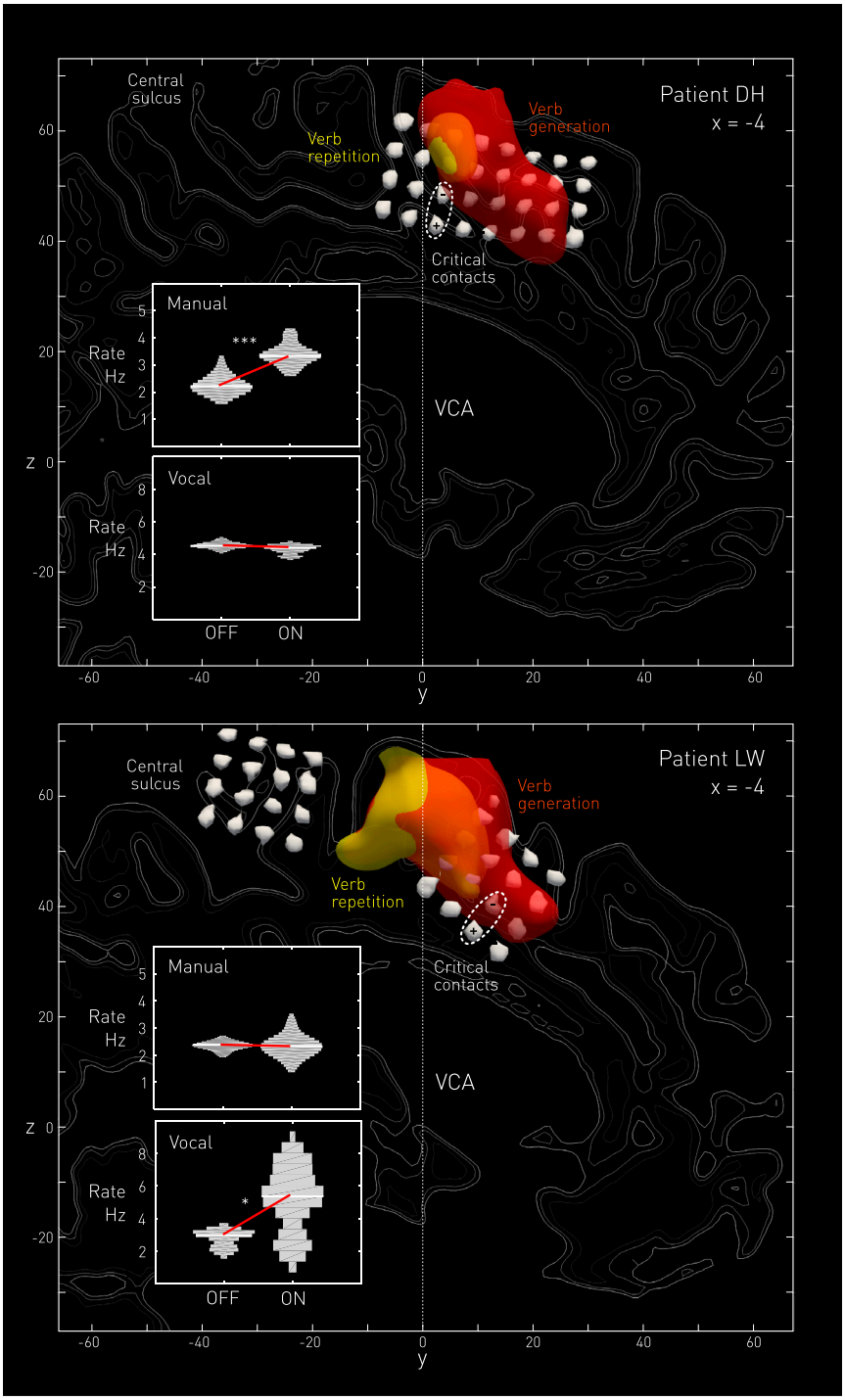


**Figure 2. Structural and Functional Localization of Stimulation Sites on the Medial Frontal Wall and Associated Behavior**

In separate panels for each patient are shown renders of the MR structural, MR functional, and CT post-electrode-implantation imaging, all non-linearly transformed into standard MNI stereotactic space by a unified normalization and segmentation procedure implemented in SPM12. For each patient, the MR structural image (a pre-implantation T1-weighted 0.94 × 0.94 × 1.1 mm acquisition from which the MNI normalization parameters were derived for all other imaging) is represented for clarity by the estimated gray matter compartment only, with isolines corresponding to the 90%, 80%, and 70% probability contours, in that order of increasing intensity, cut through a parasagittal plane at x = −4 mm. The functional imaging data, performed before implantation and derived from blocked verb repetition (yellow) or verb generation (red) compared with rest, were used to compute SPM *t*-statistic maps of significant task-related activation, which were then rigidly co-registered to the structural scan via the mean echoplanar image and subsequently transformed into MNI space. Semi-transparent contours of the clusters on the medial wall are thresholded at p = 0.05 family-wise error corrected, except for verb generation in DH where weak activation necessitated a drop in threshold to p = 0.001 uncorrected. The CT post-electrode-implantation image, a 0.43 × 0.43 × 1.2 mm acquisition, was rigidly co-registered to the pre-operative MR volume and then non-linearly adjusted by a unified normalization and segmentation procedure with the previously estimated, smoothed native space MR tissue compartments applied as priors. The non-linear adjustment was applied to compensate for the subtle but noticeable descent of the dorsal surface following craniotomy so as to improve the accuracy of contact localization in the dorsoventral plane. As with the others, this adjusted image was then transformed into MNI space using the parameters derived from the MR image, resampled to 1 × 1 × 1 mm resolution. Each grid contact was then visualized by rendering with a contour thresholded at metal density, within a region of interest enclosing the medial wall so as to exclude both bone and contacts elsewhere in the brain. The critical loci where a behavioral effect was observed are enclosed by dashed ellipses, lying on the ventral border of the pre-supplementary motor area. Note that since the stimulation current was biphasic, the polarity of the electrodes reversed at 50 Hz.

The insets show violin plots of the distributions of the reciprocals of the inter-movement intervals—essentially instantaneous frequency, in Hz—for the alternating tasks the patients performed, both manually and vocally, while the critical contacts were stimulated. The manual task consisted of self-paced, repetitive finger flexion and extension movements; the vocal task consisted of equally self-paced, repetitive single syllable vocalizations of the form "la-la-la." The red lines index the change in the locations of the distributions, showing a significant increase in behavioral frequency in the manual task for DH ($p < 0.001$, Bonferroni adjusted, marked ***) and in the vocal task for LW ($p = 0.030$, Bonferroni adjusted, marked *), consistent with effector-specific inhibition of procrastination. See also Figures S1–S3, Tables S1 and S2, and Movie S1.

the neural processes were increased, there should be a "shift" along the time axis, the slope of the function remaining unchanged. To determine which of these two alternatives best agreed with the data, we fitted LATER models where either the intercept (swivel model) or the slope (shift model) was fixed across the stimulation factor. We also estimated an

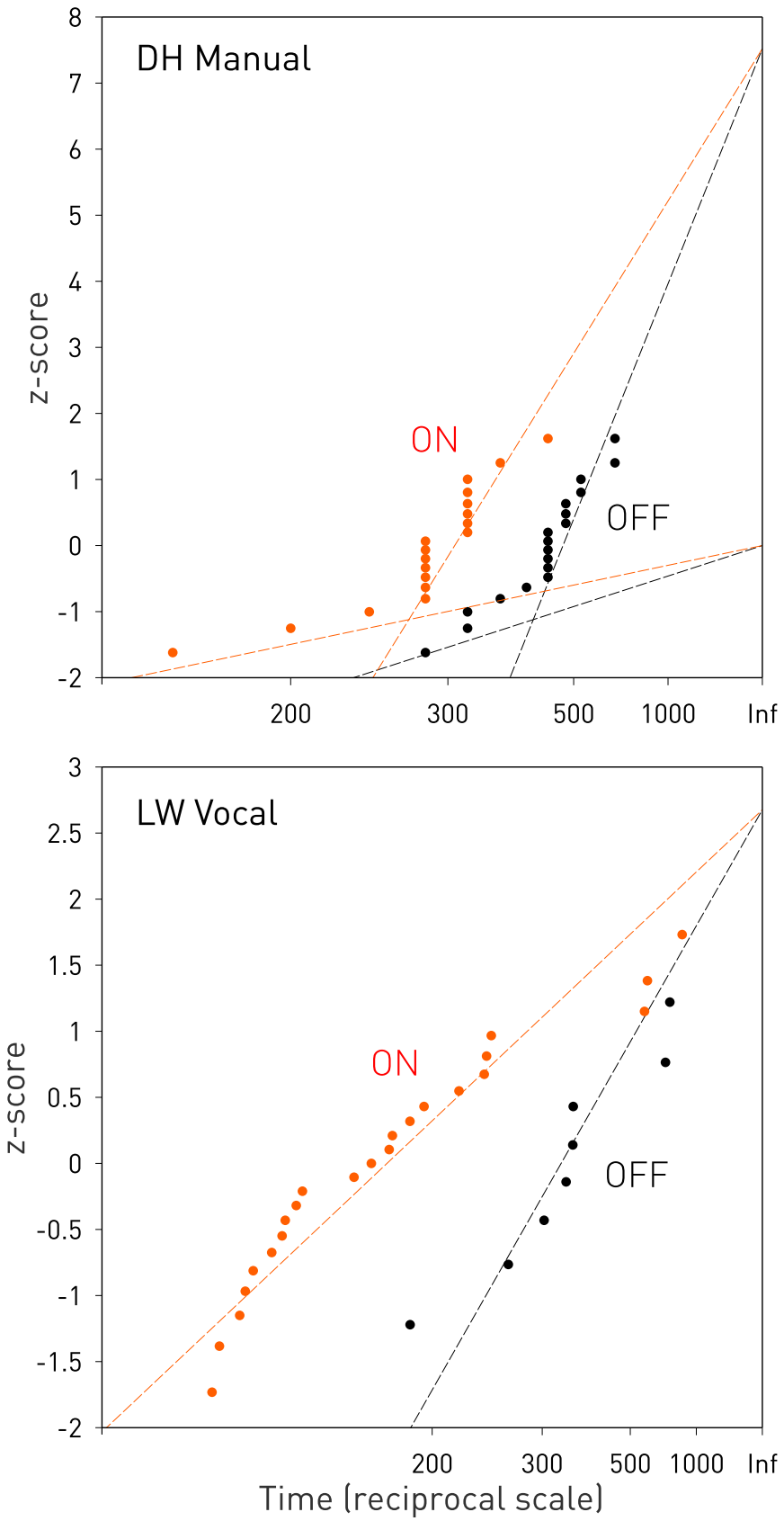


**Figure 3. LATER Analysis of Inter-movement Intervals**

Although the patients made self-paced alternating movements, it is licit to treat the inter-movement intervals as reaction times relative to an endogenous timing signal setting the individual rate of alternation. The observation catalytic of the LATER model—that reaction times show a linear relationship when plotted as their reciprocals against their cumulative (assumed Gaussian) distribution—can thus be tested on our data. Plotted here so transformed are the intervals for the electrodes where a significant effect of stimulation (in red) was observed (the manual task in DH, top, and the vocal task in LW, bottom) with time on a reciprocal scale as the abscissa and the *Z* score as the ordinate index of position within a Gaussian distribution. Maximum likelihood fits of the major components of the distributions and (only in DH where it was present) separately for the minor early components are given in dashed lines. According to the LATER model, stimulation-induced reversed procrastination predicts a change in the slope of the function, causing it to swivel around a fixed intercept, whereas acceleration of the competing processes predicts a shift to the left along the abscissa, leaving the slope unchanged. Model comparison using the BIC as the metric of modeling felicity indicated that swivel was better than shift (change in BIC = 4.82, substantial evidence). It was also better than both the unconstrained (change in BIC = 13.45, very strong evidence) and the null model (change in BIC = 32.38, very strong evidence). LATER analysis thus here supports reversed procrastination. See Supplemental Experimental Procedures for details. Note the discretization of timing data in DH is a consequence of the relatively sparse temporal sampling of standard clinical video recording (every 40 ms). LATER modeling was performed using Mike Shadlen's Reciprobit Toolbox v.1.0. See also Figures S1 and S2.

unconstrained model, where each of these parameters was allowed to vary, and a null model, where none could. Model comparison using the Bayesian information criterion (BIC) as the metric of modeling felicity indicated that swivel was better than shift (change in BIC = 4.82, substantial evidence). It was also better than both the unconstrained (change in BIC = 13.45, very strong evidence) and the null model (change in BIC = 32.38, very strong evidence). LATER not only fits the observed natural behavior here, reversed procrastination is the effect of stimulation it favors over other alternatives. Parameter estimates from the winning model indicated a relative reduction in the decision threshold by a factor of 0.65 (bootstrapped confidence intervals [CI] 0.58 to 0.78) in the motor condition and a factor of 0.56 (bootstrapped CI 0.41 to 0.72) in the vocal condition.

All race models of action naturally allow for effector specificity, for two or more action possibilities may be said to compete only to the extent to which they share an effector. The dissociation we observed may be reflective of the underlying rostrocaudal somatotopic organization of the medial wall, though the functional boundaries of vocalization-sensitive areas on the medial wall independently determined by individual fMRI as part of the clinical investigation of the patient are comparatively wide (Figure 2, red and yellow plots). The most rostral boundary of the cortex significantly activated by verb generation is clearly closer in LW than in DH to the critical stimulation contacts, but this is difficult to interpret given the smoothness of the functional data and inter-individual differences here in the task-specific BOLD signal.

What effector specificity does demonstrate, however, is that the reversed procrastination effect cannot plausibly result from a global confound such as arousal, nor from remote effects such as altered sensory feedback that would reasonably be expected to operate cross-modally. That this is fundamentally a motor phenomenon is further reinforced by the patients' own perceptions of isolated, inexplicable acceleration in their behavior, over which they otherwise felt retained overall control. Continuous, simultaneous electroencephalography during the entire procedure showed no electrophysiological evidence of ictal activity, either during or after stimulation at other intracerebral electrodes.

Equally, this was not plausibly activation—always a possibility with electrical stimulation even if the overall effect is generally disruptive—of a specific movement pattern with a specific rate of alternation, for that would not explain why it was conditional on the action the patient was executing at the time, and why the stimulated pattern was always faster than baseline. A stimulated movement would be expected to be not only simple and monophasic, rather than complex, coordinated, and repetitive as here, but also morphologically identical, replacing the preceding action, rather than conditionally altering just one feature of it: its speed of execution. Repeated activation of a single movement component should have resulted in a tonic response, uninterrupted by its previously alternating rival, completely extinguishing the repetitive behavior in favor of just one component of it. Even if theoretically possible, at 50 Hz, the stimulation frequency was far too high to give rise to alternating movements of the observed frequency by resonance or interference with endogenous neural oscillations: that would in any rate have predicted a fixed resultant frequency across all stimulated conditions, not the increase from a self-determined baseline we observed. Finally, outwardly and as perceived by the patients themselves, this was morphologically essentially normal behavior, for it largely retained the features preceding its disruption, including the capacity to stop it altogether.

An intriguing alternative possibility, however, is that this is a manifestation of stochastic resonance within the human motor domain, a more complex phenomenon where non-linearities in the system cause the addition of noise not to degrade but to amplify the underlying neural signal [22]. Given that the effects here were observed at relatively high stimulation intensities, thought substantially to disrupt underlying activity, not just to add a degree of noise, this seems unlikely [18]. Note that a mechanism relying on a lower degree of disruption at a more distant locus where the intensity is lower, in ''penumbra'' fashion, is unlikely to explain our observations, for the penumbra will inevitably be larger than the point of stimulation, and so would likely have been comparably induced by stimulation of neighboring positions on the implanted grids. In any event, it is only within the context of a race model that enhancement of the activity of competing neuronal coalitions could plausibly result in a rate of behavior faster than the subject intends.

Disruptive stimulation of the present scale—a spheroid a few millimeters in diameter [23]—is not easily related to microstimulation in non-human primates, where the scale is finer, likely confined to a narrower subset of competing neuronal ensembles, and the currents lower, with potentially facilitatory effects. Procrastination here would thus be enhanced rather than reversed, resulting in delay, not acceleration. In the context of saccades, where saccadic direction may be taken as a marker of task specificity, facilitatory stimulation of the pre-supplementary motor area has been associated with relatively direction-insensitive increased latency, in broad agreement with our observations [6, 24, 25]. Nonetheless, the timing of stimulation in these studies strongly modulated the effect on latency, including reversing it when applied before a saccade was cued. In the closely related supplementary eye field, greater task specificity has been observed, including facilitated acceleration [25–28], though it is interesting that controlled, memory-guided, highly contextual behaviors that more heavily engage medial structures have been more often delayed than accelerated.

Direct, interventional access to human cortex can only ever be justified clinically: the biological picture thereby framed is inevitably refracted through the lens of pathology. Although this sets a constraint on generalizing to wholly normal populations, we should note these patients were affected by a focal neurological disorder with predominantly intermittent functional manifestations that were absent during the study. Moreover, neither patient showed clinical evidence of any discernible impairments in their capacity for voluntary action.

Overall, disruption of a fundamental feature of decision-making, long predicted by race models of action, appears to be the most plausible explanation for the stimulation-induced phenomena in our patients. This observation reinforces the remarkable felicity of race models in understanding how we select our actions and urges the pursuit of their wider ramifications across the broader neural organization of voluntary action.

## SUPPLEMENTAL INFORMATION

Supplemental Information includes Supplemental Experimental Procedures, three figures, two tables, and one movie and can be found with this article online at http://dx.doi.org/10.1016/j.cub.2016.08.016.

## AUTHOR CONTRIBUTIONS

A.J. and B.D. contributed equally to the study as joint first authors. A.J., B.D., and P.N. conceived, conducted, analyzed, and reported the study. C.S. and A.W.M. contributed to the execution of the study in relation to behavioral testing and neurosurgical procedures, respectively.

## ACKNOWLEDGMENTS

Informed consent for research analysis of the clinical data was obtained prior to testing following our standard clinical and institutional guidelines. This work was undertaken at UCLH/UCL, which receives a portion of funding from the Department of Health's NIHR Biomedical Research Centres funding scheme. B.D. receives funding from the NIH-National Institute of Neurological Disorders and Stroke (U01-NS090407), the Centre for SUDEP Research, and Epilepsy Research UK (PGE 1302). A.J. is funded by the Guarantors of Brain. P.N. is funded by the Wellcome Trust and the Department of Health (HICF-R9-501) and the UCLH National Institute of Health Research Biomedical Research Centre. We are grateful to Professor John Ashburner for advice on image processing methodology.

Received: April 19, 2016
Revised: July 18, 2016
Accepted: August 5, 2016
Published: October 20, 2016

## REFERENCES

1. Mainen, Z.F., and Sejnowski, T.J. (1995). Reliability of spike timing in neocortical neurons. Science *268*, 1503–1506.
2. Corey, D.P., and Hudspeth, A.J. (1979). Response latency of vertebrate hair cells. Biophys. J. *26*, 499–506.
3. Nachev, P., and Hacker, P. (2014). The neural antecedents to voluntary action: a conceptual analysis. Cogn. Neurosci. *5*, 193–208.
4. Verbruggen, F., and Logan, G.D. (2009). Models of response inhibition in the stop-signal and stop-change paradigms. Neurosci. Biobehav. Rev. *33*, 647–661.
5. Schall, J.D. (2004). On building a bridge between brain and behavior. Annu. Rev. Psychol. *55*, 23–50.
6. Hikosaka, O., and Isoda, M. (2010). Switching from automatic to controlled behavior: cortico-basal ganglia mechanisms. Trends Cogn. Sci. *14*, 154–161.
7. Carpenter, R.H.S. (1981). Oculomotor procrastination. In Eye Movements: Cognition and Visual Perception, D.F. Fisher, R.A. Monty, and J.W. Senders, eds. (L. Erlbaum Associates), pp. 237–246.
8. Carpenter, R.H.S., and Williams, M.L.L. (1995). Neural computation of log likelihood in control of saccadic eye movements. Nature *377*, 59–62.
9. Gold, J.I., and Shadlen, M.N. (2007). The neural basis of decision making. Annu. Rev. Neurosci. *30*, 535–574.
10. Bogacz, R., Brown, E., Moehlis, J., Holmes, P., and Cohen, J.D. (2006). The physics of optimal decision making: a formal analysis of models of performance in two-alternative forced-choice tasks. Psychol. Rev. *113*, 700–765.
11. Ratcliff, R., and McKoon, G. (2008). The diffusion decision model: theory and data for two-choice decision tasks. Neural Comput. *20*, 873–922.
12. Picard, N., and Strick, P.L. (1996). Motor areas of the medial wall: a review of their location and functional activation. Cereb. Cortex *6*, 342–353.
13. Nachev, P., Kennard, C., and Husain, M. (2008). Functional role of the supplementary and pre-supplementary motor areas. Nat. Rev. Neurosci. *9*, 856–869.
14. Grinband, J., Savitskaya, J., Wager, T.D., Teichert, T., Ferrera, V.P., and Hirsch, J. (2011). The dorsal medial frontal cortex is sensitive to time on task, not response conflict or error likelihood. Neuroimage *57*, 303–311.
15. Penfield, W., and Rasmussen, T. (1950). The Cerebral Cortex of Man: A Clinical Study of Localization of Function (Macmillan).
16. Borchers, S., Himmelbach, M., Logothetis, N., and Karnath, H.-O. (2011). Direct electrical stimulation of human cortex - the gold standard for mapping brain functions? Nat. Rev. Neurosci. *13*, 63–70.
17. Kovac, S., Scott, C.A., Maglajlija, V., Toms, N., Rodionov, R., Miserocchi, A., McEvoy, A.W., and Diehl, B. (2014). Comparison of bipolar versus monopolar extraoperative electrical cortical stimulation mapping in patients with focal epilepsy. Clin. Neurophysiol. *125*, 667–674.
18. Mandonnet, E., Winkler, P.A., and Duffau, H. (2010). Direct electrical stimulation as an input gate into brain functional networks: principles, advantages and limitations. Acta Neurochir. (Wien) *152*, 185–193.
19. Carpenter, R.H.S., and McDonald, S.A. (2007). LATER predicts saccade latency distributions in reading. Exp. Brain Res. *177*, 176–183.
20. Roos, J.C.P., Calandrini, D.M., and Carpenter, R.H.S. (2008). A single mechanism for the timing of spontaneous and evoked saccades. Exp. Brain Res. *187*, 283–293.
21. Reddi, B.A., and Carpenter, R.H.S. (2000). The influence of urgency on decision time. Nat. Neurosci. *3*, 827–830.
22. Gammaitoni, L., Hänggi, P., Jung, P., and Marchesoni, F. (1998). Stochastic resonance. Rev. Mod. Phys. *70*, 223–287.
23. Chaturvedi, A., Luján, J.L., and McIntyre, C.C. (2013). Artificial neural network based characterization of the volume of tissue activated during deep brain stimulation. J. Neural Eng. *10*, 056023.
24. Isoda, M. (2005). Context-dependent stimulation effects on saccade initiation in the presupplementary motor area of the monkey. J. Neurophysiol. *93*, 3016–3022.
25. Yang, S.N., Heinen, S.J., and Missal, M. (2008). The effects of microstimulation of the dorsomedial frontal cortex on saccade latency. J. Neurophysiol. *99*, 1857–1870.
26. Stuphorn, V., and Schall, J.D. (2006). Executive control of countermanding saccades by the supplementary eye field. Nat. Neurosci. *9*, 925–931.
27. Berdyyeva, T.K., and Olson, C.R. (2014). Intracortical microstimulation of supplementary eye field impairs ability of monkeys to make serially ordered saccades. J. Neurophysiol. *111*, 1529–1540.
28. Kunimatsu, J., and Tanaka, M. (2012). Alteration of the timing of self-initiated but not reactive saccades by electrical stimulation in the supplementary eye field. Eur. J. Neurosci. *36*, 3258–3268.

**Current Biology, Volume *26***

## Supplemental Information

# Reversed Procrastination by Focal Disruption of Medial Frontal Cortex

**Ashwani Jha, Beate Diehl, Catherine Scott, Andrew W. McEvoy, and Parashkev Nachev**

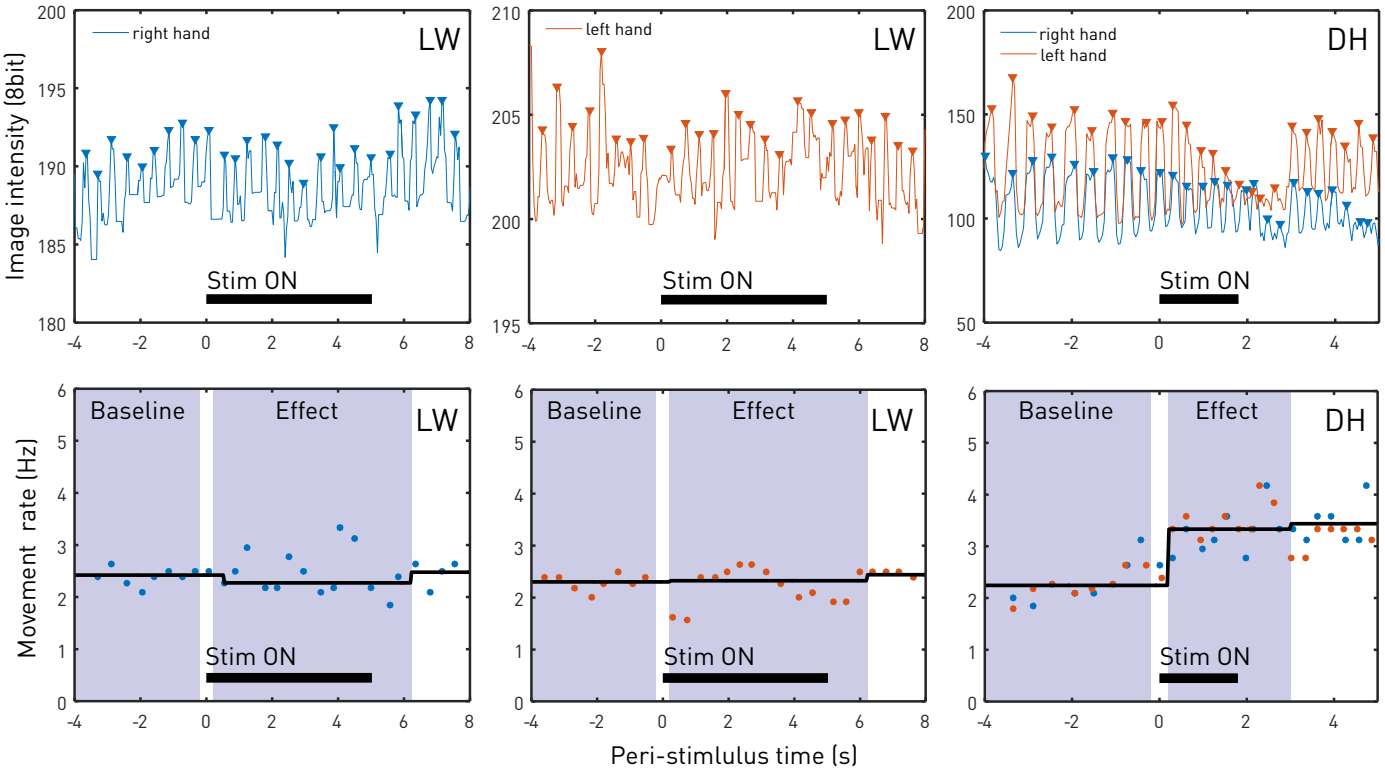


**Figure S1.** Parameterisation of manual movements during cortical stimulation. Related to Figures 2 and 3. The top row of plots shows the 8-bit greyscale image intensity values within the region of interest capturing the patient's fingers, for each hand, as a function of time, with the stimulation period marked in black above the abscissa. The triangles show automatically identified peaks. The bottom row shows the inter-peak intervals converted to instantaneous frequency by taking, for each point, the reciprocal of the average time interval between the preceding two movements. In grey are the windows defining the intervals included in the baseline and stimulation analyses. The black line is a 1st order spline with breakpoints at the window edges robustly fitted to the data for illustration. Note the clear change in manual task performance for DH, but not LW.

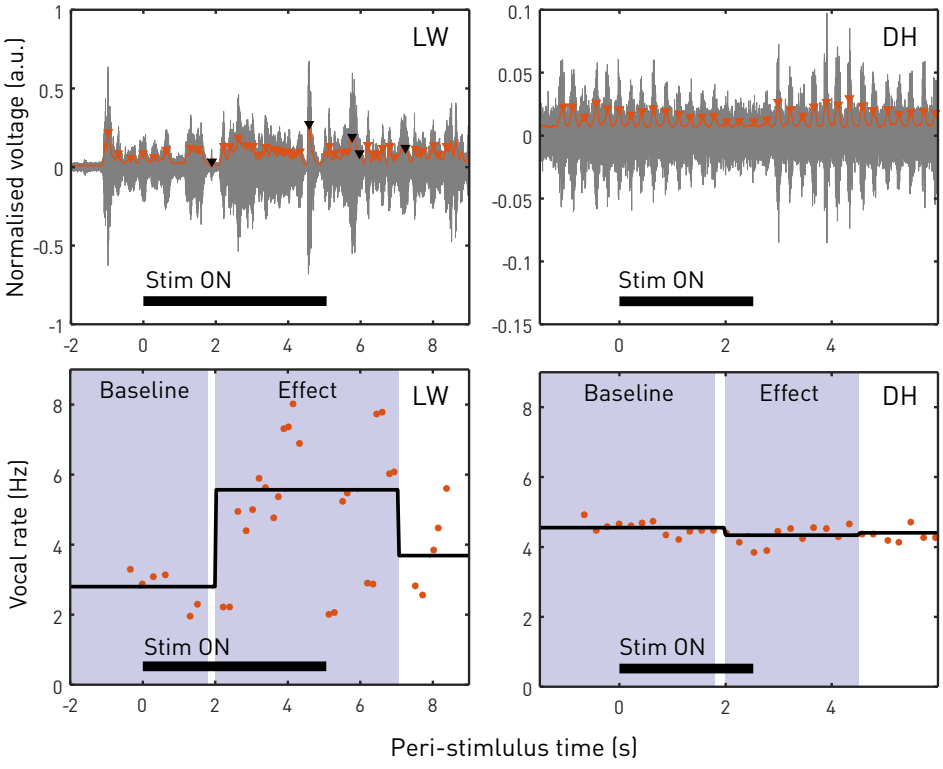


**Figure S2.** Parameterisation of vocal movements during cortical stimulation. Related to Figures 2 and 3. The top row of plots shows the high-pass filtered audio track voltage (in gray, normalised with 16 bit precision to arbirary units in the range -1:1), with the stimulation period marked in black above the abscissa. In red is the upper root mean square envelope of the signal, of which the red triangles show automatically identified peaks. Black triangles were manually removed artefacts. The bottom row shows the inter-peak intervals converted to instantaneous frequency as in the manual case, with 1st order splines identically fitted. Note the clear change in vocal task performance for LW, but not DH.

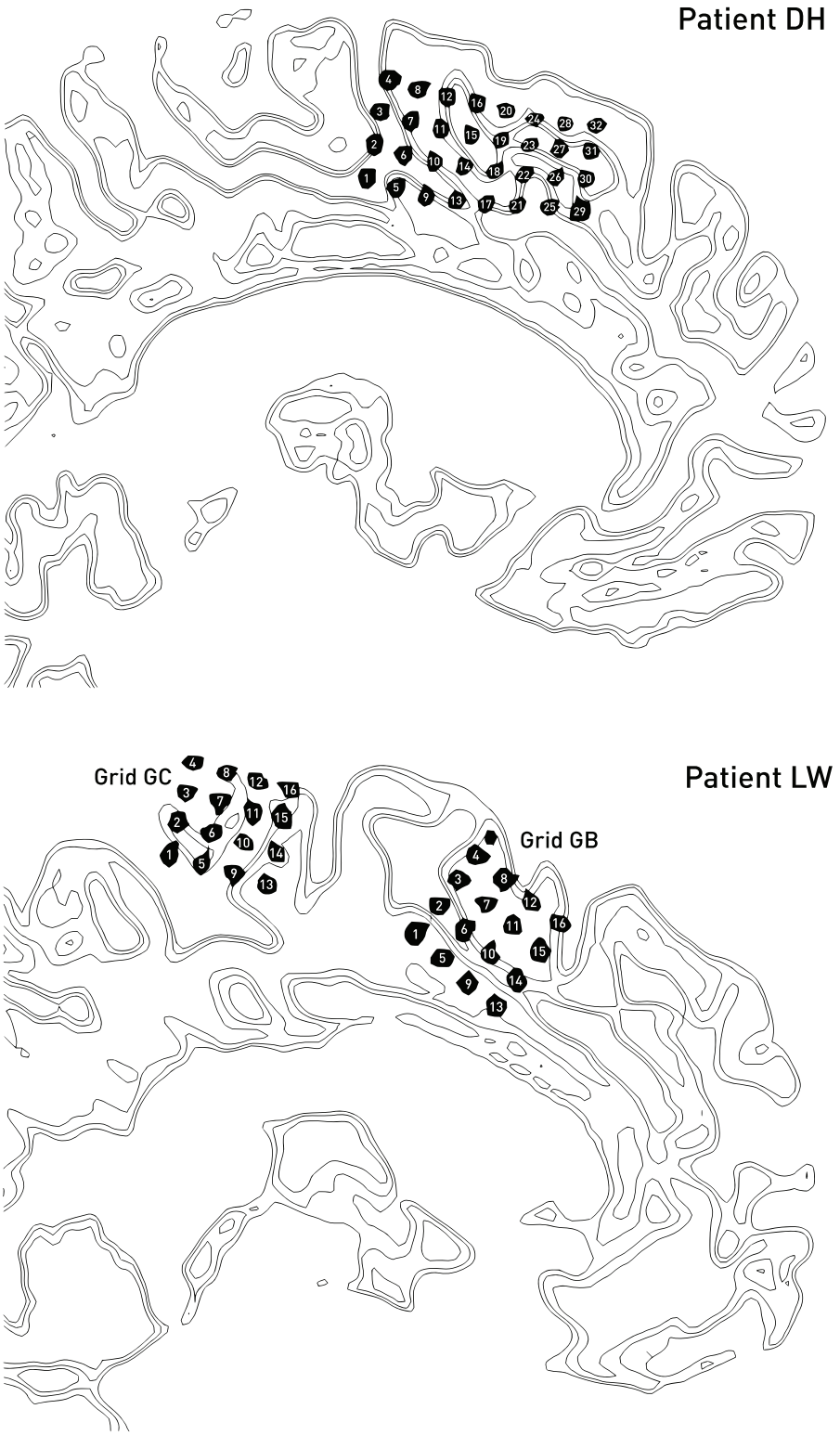


Figure S3. Electrode grid montages. Related to Figure 2. The labelling of electrodes in the relevant intracranial grids in participants DH (upper panel) and LW (lower panel) is shown. Stimulation effects at various bipolar electrode configurations within these grids are given in Table S2.

**Table S1.** Clinical details. Related to Figure 2.

| Details | DH | LW |
|---|---|---|
| Age (at onset) | 41 (29) | 36 (12) |
| Handedness | R | R |
| Gender | M | F |
| Main seizure types | Atonic; tonic/clonic | Right arm/leg tonic; Atonic |
| Anti-epileptic medications | Lacosamide 100mg bd<br>Zonisamide 150mg bd | Tegretol Retard 700mg/800mg<br>Clobazam 10mg<br>Diazepam 5-10mg |
| Suspected zone | Left frontal | Left frontal |
| Language | Left dominant (fMRI) | Left dominant (fMRI) |
| Subdural grids (High density: 5 mm, centre-to-centre; regular density: 10 mm centre-to-centre | **Medial wall:**<br>High density: one 4x8, one 4x4.<br><br>**Lateral wall:**<br>8x8 frontoparietal,<br>2x8 anterior superior frontal gyrus,<br>1x6 middle frontal gyrus,<br>Two 1x6 inferior frontal gyrus. | **Medial wall:**<br>High density: one 4x4<br>1x6 strip.<br><br>**Lateral wall:**<br>8x8 frontoparietal |
| Stimulation currents during tasks | **Manual (bilateral):** 1mA<br>**Vocal:** 3mA | **Manual (left):** 3mA<br>**Manual (right):** 3.5mA<br>**Vocal:** 4mA |

Table S2. Summary of stimulation effects (critical sites in grey). Related to Figure 2.

| Subject | Contact pair | | Task | Subjective effects | Stimulation parameters | | Syllables or taps | | Behavioural rate (Hz) | | | Statistics (*t*-test) | | |
|---|---|---|---|---|---|---|---|---|---|---|---|---|---|---|
| | | | | | *mA* | *s* | *Pre* | *Post* | *Pre* | *Post* | *Δ* | *df* | *t* | *p* |
| LW | 9 | 10 | 'lala' | None | 4 | 5.06 | 7 | 24 | 2.77 | 5.14 | 2.37 | 27 | -2.90 | 0.030 |
| DH | 9 | 10 | 'tata' | None | 3 | 2.52 | 13 | 12 | 4.55 | 4.32 | -0.23 | 21 | 2.42 | 0.980 |
| LW | 9 | 10 | Tap (l) | None | 3 | 5.03 | 10 | 16 | 2.34 | 2.33 | -0.01 | 43 | 0.05 | 1.000 |
| LW | 9 | 10 | Tap (r) | None | 3.5 | 5.03 | 10 | 13 | | | | | | |
| DH | 9 | 10 | Tap (l&r) | None | 1 | 1.62 | 17 | 19 | 2.27 | 3.39 | 1.12 | 32 | -8.803 | <0.001 |
| DH | 32 | 31 | Reading | None | 3 | 2.25 | 14 | 8 | 3.07 | 3.30 | 0.23 | 18 | -0.54 | 0.60 |
| DH | 30 | 29 | Reading | None | 3 | 2.06 | 13 | 7 | 3.97 | 3.49 | -0.48 | 16 | 0.65 | 0.53 |
| DH | 28 | 27 | Reading | None | 3 | 2.78 | 12 | 10 | 3.30 | 3.68 | 0.38 | 18 | -0.63 | 0.54 |
| DH | 26 | 25 | Reading | None | 3 | 2.57 | 12 | 7 | 2.84 | 2.37 | -0.47 | 15 | 1.09 | 0.29 |
| DH | 24 | 23 | Reading | None | 3 | 2.82 | 15 | 4 | 3.95 | 3.86 | -0.09 | 15 | 0.11 | 0.92 |
| DH | 22 | 21 | Reading | None | 3 | 3.07 | 12 | 9 | 3.53 | 3.10 | -0.43 | 17 | 0.66 | 0.52 |
| DH | 18 | 17 | Reading | None | 3 | 2.57 | 13 | 5 | 3.45 | 4.20 | 0.74 | 14 | -0.79 | 0.44 |
| DH | 16 | 15 | Reading | Speech | 3 | 2.2 | 11 | 3 | Too few syllables | | | | | |
| DH | 14 | 13 | Reading | None | 3 | 2.81 | 11 | 11 | 3.39 | 3.63 | 0.25 | 18 | -0.40 | 0.69 |
| DH | 12 | 11 | Reading | None | 3 | 2.65 | 13 | 8 | 3.27 | 2.73 | -0.55 | 17 | 1.24 | 0.23 |
| DH | 8 | 7 | Reading | Sensory | 2 | 1.06 | 11 | 1 | Too few syllables | | | | | |
| DH | 6 | 5 | Reading | Sensory | 2 | 1.38 | 10 | 1 | Too few syllables | | | | | |
| DH | 4 | 3 | Reading | None | 1 | 2.7 | 8 | 8 | 3.11 | 2.63 | -0.48 | 12 | 0.89 | 0.39 |
| DH | 2 | 1 | Reading | None | 3 | 3.12 | 8 | 7 | 2.13 | 2.36 | 0.23 | 11 | -0.46 | 0.65 |
| DH | 3 | 2 | Reading | Sensory | 3 | 2.99 | 11 | 8 | 2.71 | 3.07 | 0.36 | 15 | -0.48 | 0.64 |
| DH | 32 | 31 | Tapping | None | 3 | 2.78 | 3 | 20 | Too few taps | | | | | |
| DH | 30 | 29 | Tapping | None | 3 | 2.85 | 8 | 20 | 2.30 | 2.45 | 0.15 | 24 | -1.28 | 0.21 |
| DH | 28 | 27 | Tapping | None | 3 | 2.62 | 1 | 17 | Too few taps | | | | | |
| DH | 26 | 25 | Tapping | None | 3 | 2.66 | 4 | 17 | Too few taps | | | | | |
| DH | 24 | 23 | Tapping | None | 3 | 1.66 | 16 | 1 | Too few taps | | | | | |
| DH | 22 | 21 | Tapping | None | 3 | 2.91 | 1 | 20 | Too few taps | | | | | |
| DH | 18 | 17 | Tapping | None | 3 | 2.27 | 3 | 17 | Too few taps | | | | | |
| DH | 14 | 13 | Tapping | None | 3 | 3.12 | 1 | 22 | Too few taps | | | | | |
| DH | 12 | 11 | Tapping | None | 3 | 3.35 | 1 | 24 | Too few taps | | | | | |
| DH | 8 | 7 | Tapping | None | 2 | 1.32 | 1 | 13 | Too few taps | | | | | |
| DH | 6 | 5 | Tapping | None | 3 | 0.96 | 3 | 10 | Too few taps | | | | | |
| DH | 3 | 2 | Tapping | None | 3 | 2.55 | 1 | 19 | Too few taps | | | | | |
| LW-GC | 4 | 8 | At rest | Sensory foot | 3 | | | | | | | | | |
| LW-GC | 12 | 8 | At rest | Sensory foot | 3 | | | | | | | | | |
| LW-GC | 12 | 16 | At rest | Motor foot | 3 | | | | | | | | | |
| LW-GC | 3 | 7 | At rest | Motor foot | 2 | | | | | | | | | |
| LW-GC | 11 | 7 | At rest | Motor foot | 2 | | | | | | | | | |
| LW-GC | 9 | 13 | At rest | Sensory foot | 2 | | | | | | | | | |
| LW-GC | 13 | 14 | At rest | Motor arm | 3 | | | | | | | | | |
| LW-GC | 14 | 15 | At rest | Motor arm | 3 | | | | | | | | | |
| LW-GC | 15 | 16 | At rest | Motor arm | 3 | | | | | | | | | |
| LW-GC | 10 | 11 | At rest | Motor leg | 2 | | | | | | | | | |
| LW-GC | 11 | 12 | At rest | Sensory foot | 2 | | | | | | | | | |
| LW-GC | 5 | 6 | At rest | Sensory face | 1 | | | | | | | | | |
| LW-GC | 6 | 7 | At rest | Motor face | 2 | | | | | | | | | |
| LW-GC | 7 | 8 | At rest | Motor foot | 2 | | | | | | | | | |
| LW-GC | 1 | 2 | At rest | Motor foot | 3 | After-discharges | | | | | | | | |
| LW-GC | 2 | 3 | At rest | Sensory foot | 3 | | | | | | | | | |
| LW-GC | 3 | 4 | At rest | Sensory foot | 1 | | | | | | | | | |
| LW-GB | 13 | 14 | At rest | Sensory foot | 3 | | | | | | | | | |
| LW-GB | 15 | 16 | At rest | Sensory foot | 3.5 | | | | | | | | | |
| LW-GB | 14 | 15 | At rest | Motor foot | 3.5 | | | | | | | | | |
| LW-GB | 5 | 6 | At rest | Motor arm | 4 | | | | | | | | | |
| LW-GB | 6 | 7 | At rest | Motor arm | 4 | | | | | | | | | |
| LW-GB | 7 | 8 | At rest | None | 3 | | | | | | | | | |
| LW-GB | 1 | 2 | At rest | Motor arm | 3 | | | | | | | | | |

# Supplemental Experimental Procedures

## Participants

We studied two patients with non-lesional, medically-refractory, focal epilepsy during their clinical evaluation for potential neurosurgical treatment. The patients were admitted to the Sir Jules Thorn Telemetry Unit at the National Hospital for Neurology and Neurosurgery, London, UK. While no clear epileptic focus had been identified in either patient—hence requiring invasive neurophysiological study—the clinical picture and non-invasive neurophysiology included the left medial frontal wall within the range of possible targets. Both patients therefore underwent temporary implantation of subdural grids on the medial frontal cortical wall amongst other areas. The precise locations differed between the two patients for clinical reasons, but comparable coverage of the medial aspect of the superior frontal gyrus was obtained. The clinical details are given in Table S1.

The standard clinical protocol to formulate a hypothesis for seizure focus localisation includes the following: clinical assessment to identify seizure types and evolution of the epilepsy over time, scalp video telemetry to determine interictal and ictal source localisation of epileptic activity, structural and functional imaging including FDG-PET to determine presence of a lesion, functional MRI to determine language lateralisation, and neuropsychiatric and neuropsychological assessment to determine impact of the epilepsy and risk for resection. The decision whether or not a patient is a candidate for potentially curative resective surgery is made during a multidisciplinary team meeting, and whether or not intracranial EEG is first required for more precise focus localisation and/or mapping of eloquent cortex. A detailed plan for implantation of the intracranial electrodes is then devised. The intracranial neurophysiological evaluation relies on precise localisation of the electrode position by review of pre-implantation MRI fused to the post-implantation CT. Continuous video EEG telemetry identifies intracranial epileptform activity both between and during seizures. Further, direct electrical cortical stimulation of each implanted electrode is performed to map eloquent cortex and to predict the behavioural consequences should the region be resected.

Below we set out the aspects of the protocol relevant to our study.

Informed consent for research analysis of the clinical data was obtained prior to testing following our standard clinical guidelines. The patient's identifying initials here bear no relation to their own, and all plausibly identifying information has been removed.

*Clinical details*

LW: At the time of evaluation, LW was a 36 year-old, right-handed woman with frequent (>10 a day) disabling seizures dating from the age 12, characterised by right leg and arm tonic seizures that occasionally generalised, as well as rarer atonic seizures, including complete inability to move with preserved consciousness. Scalp EEG supported a left frontal or

frontocentral focus with left frontocentral interictal spikes; seizures showed a left frontocentral ictal pattern. The neurological examination was unremarkable. Neuropsychometric assessment did not reveal any significant cognitive deficits. An FDG-PET scan showed no areas of significant brain hypometabolism.

DH: At the time of evaluation, DH was a 41 year-old right-handed man with atonic seizures and generalised tonic clonic seizures dating from the age of 29. Scalp EEG had revealed slowing, but no spikes, over the left frontocentral region. Numerous seizures with atonia and right head version followed by a right arm clonic seizure were also recorded, and ictal EEG implicated the medial frontal region. Neurological examination was normal. Neurocognitive assessment showed mild deficits supportive of dominant frontal lobe involvement. An FDG-PET scan was unremarkable.

Language fMRI studies revealed left language dominance in both patients.

## Structural imaging

*Data acquisition*

The same protocol was followed in both patients. Pre-operatively, a whole-brain, T1-weighted, magnetic resonance imaging of resolution 0.94x0.94x1.1mm resolution was acquired on a 3T General Electric Excite HDx scanner (General Electric, Milwaukee, WI, USA) using an eight-channel array head coil for reception and the body coil for transmission, with standard imaging gradients (maximum strength 40 mT/m and slew rate 150 T/m/s). Post-electrode implantation, the patients underwent an uncontrasted, whole-head, CT scan of resolution 0.43x0.43x1.2mm. (SOMATOM Definition 128-slice, Siemens Healthcare GmbH, Erlangen, Federal Republic of Germany). LW's neurophysiological study was carried out 4 days after the post-implantation CT scan. Since DH's neurophysiological study was carried out 4 weeks after the initial CT scan, we used instead a later scan of the same parameters, carried out within 3 days of stimulation.

*Analysis*

We sought to determine as precisely as the data allowed the location of the stimulation sites, both in relation to the patient's individual cortical anatomy, and in standard stereotactic space. This required two forms of image registration: a native space, within-subject registration of the post-implantation CT to the pre-implantation MRI, and a MNI space, template registration of the MRI, applying the derived parameters so as secondarily to warp the natively registered CT into the same space.

*CT-MRI registration*

Ordinarily, within-subject registration of one imaging modality against another requires only an affine transform, for the underlying morphology of the brain is the same. Where a craniotomy has been performed, however, a degree of non-linear adjustment is necessary to

compensate for the minor but significant distortions opening the skull introduces. This is challenging in the context of post-implantation CT because of the relative poverty of tissue contrast and the presence of electrode artefact. Nonetheless, since the routine post-operative dural collections principally responsible for the distortion cause very smooth deformations, it is possible to introduce sufficient constraint into the non-linear step to ensure the transformation remains biologically plausible. Here we develop a novel approach to performing non-linear CT-MRI registration, and validate it in our two patients with the aid of independently identified anatomical landmarks. Unless otherwise indicated, all operations were performed within SPM12 (http://www.fil.ion.ucl.ac.uk/spm/), running in Matlab R13b (http://uk.mathworks.com/), on a 64-bit machine under Windows 7 SP1. The procedure was identical for each patient.

CT PRE-PROCESSING: First, a rigid body coregistration to the standard SPM12 tissue probability map was performed based on normalised mutual information with adjustment from a Procrustes analysis weighted by the white and grey matter compartments. This placed the scan in rigid register with the MNI template space. So as to focus subsequent processing on tissue-relevant contrast, an identical copy of the scan was windowed so as to zero all voxels outside the range of 0 to 100 Hounsfield units. This was then filtered with an Oracle-based 3D discrete cosine transform filter[S1] to enhance tissue contrast. All subsequent operations were performed on this image, and the final transformation was replicated on the original image at the end.

MR PRE-PROCESSING: As for the CT, a rigid body coregistration to the standard SPM12 tissue probability map was performed based on normalised mutual information with adjustment from a Procrustes analysis weighted by the white and grey matter compartments. This placed the scan in rigid register with the MNI template space, and also with the CT. The scan was then resliced using 4$^{th}$ degree *b*-spline interpolation to the same bounding box and voxel size as the CT. SPM12's standard unified segmentation and normalisation procedure, with default parameters, was used to generate segmented compartments in native space for each of the standard 6 tissue classes, as well as a set of parameters for non-linear transformation into MNI space of this and any other image in register with it.

LANDMARK ANNOTATION: A set of 73 anatomical landmarks was manually and independently applied to each scan by a trained neurologist (PN) with the aid of MIPAV's triplanar visualisation and volume-of-interest tools (http://mipav.cit.nih.gov/). In common with established practice[S2], the landmarks fell into characteristic planes established by the anterior commissure (AC) – posterior commissure (PC) alignment achieved in the initial rigid body registration to MNI space, as follows:

Axial plane of the corpus callosum (CC) (separately for each hemisphere): lateral ventricle anterior, caudate nucleus anterior, caudate nucleus posterior, putamen anterior, putamen medial, putamen posterior, insula anterior, insula posterior, and lateral ventricle posterior.

Coronal plane through AC (separately for each hemisphere except for AC itself): lateral ventricle superior, lateral ventricle inferior, caudate superior, putamen superior, putamen inferior, globus pallidus medial, insula superior, and insula inferior.

Mid-sagittal plane: anterior cerebrum (AC-PC plane), paracingulate gyrus anterior (AC-PC plane), cingulate gyrus anterior (AC-PC plane), cerebrum posterior (AC-PC plane), corpus callosum anterior, corpus callosum posterior, corpus callosum genu angle, corpus callosum tip of genu, corpus callosum splenium centre, corpus callosum splenium posterior tip, anterior cerebrum (CC plane), paracingulate gyrus anterior (CC plane), cingulate gyrus anterior (CC plane), cerebrum posterior (CC plane), thalamus centre, cerebrum superior (AC coronal plane), corpus callosum superior (AC coronal plane), corpus callosum inferior (AC coronal plane), corpus callosum superior (PC coronal plane), corpus callosum inferior (PC coronal plane), calcarine fissure-parietooccipital fissure, parietooccipital fissure-hemisphere margin, calcarine fissure-hemisphere margin.

Lateral parasagittal planes (through insula, separately for left and right): anterior horizontal ramus of Sylvian fissure-Sylvian fissure, anterior ascendant ramus of Sylvian fissure-Sylvian fissure, inferior frontal fissure-hemisphere margin, precentral fissure-hemisphere margin, central fissure-hemisphere margin, postcentral fissure-hemisphere margin, Sylvian fissure posterior, Jensen's fissure-hemisphere margin.

Each set of landmarks was used to generate a volume image in register with, and of the same dimensions as, its corresponding scan. Any transformation applied to the scan could then be identically applied to the landmark image, allowing direct, unbiased quantification of the fidelity of registration. Registration error was indexed as the root mean squared distance (and its standard deviation) across all landmarks, taking the MR scan as the reference and each transformed CT scan as the test. The baseline registration error—the difference between the sets of landmarks following the initial rigid registration—was 3.12 mm (std=1.63 mm) for DH and 4.68 mm (std=2.07 mm) for LW.

NON-LINEAR REGISTRATION OF CT TO MR: The relatively small mean error—only a few millimetres—suggests only relatively minor non-linear adjustment is necessary. Here we performed this adjustment by applying SPM12's unified segmentation and normalisation procedure on the windowed, filtered CT scan, but instead of using the standard MNI space template tissue compartments as tissue prior probability maps we used the individual MR-derived tissue compartments in *native* space. The resultant transformation is therefore not into standard stereotactic space but rather the native space of the T1 (which the CT already shares), adjusted to introduce some conformity with the native MR tissue segmentation. Other than removing the affine registration step and any bias correction, the parameters of the algorithm were otherwise as default in SPM12. Note that since SPM12's routine involves explicitly modelling anomalous signal, this adjustment was robust to the artefact created by the metal grids. Inspection of the tissue compartments from the CT segmentation showed that the critical grey and white matter partitions were not significantly contaminated by the artefact, though of course it did limit the extent to which the neighbouring tissues could

materially contribute to the deformation. So as to optimise the degree of laxity in the transformation, the procedure was repeated with different levels of smoothing applied to the MR tissue compartments before they were used as priors, in the range of a Gaussian kernel of 1 to 8 mm full width half maximum, in 1 mm steps. The deformation field describing the transformation was applied both to the CT and its corresponding landmark image. Tested against the MR, the smallest landmark error was found with a kernel of 4mm width: this was therefore used in the final analysis. The final root mean square errors were 3.09 mm (std=1.35 mm) for DH, and 3.88 (std=2.32 mm) for LW.

Note that the registration process itself *does not use the landmarks in any way.* Optimising the transformation by refining the degree of smoothing of the priors is therefore not in any danger of creating an artificial overfit to the data, as the landmark proximity reflects—but does not drive—the process.

NORMALISATION (TRANSFORMATION INTO MNI SPACE): The deformation field estimated from the MR scan segmentation and normalisation was applied to the grey matter compartment of the MR image, producing a probabilistic map of grey matter transformed in standard MNI space. Since the MR was a standard high-resolution, volumetric, unlesioned scan, there were no grounds to suspect the quality of registration, and no need for landmark analysis of this step. The same deformation field was used to transform the final MR-registered CT into the same space. Both transformed images were resliced to 1mm isotropic voxels. The output of this stage was thus two MNI transformed maps: one of MR-derived, grey matter, and another of the CT-derived electrode locations.

*Visualisation*

So as to visualise the location of the electrodes, the normalised images were rendered in ParaView (http://www.paraview.org/) as thresholded 3D contours. For the grey matter image, three contours were created for tissue probability values of 0.9, 0.8, and 0.7. A parasagittal slice cutting through the brain at x = -4 thus created a set of isolines as a probabilistic guide to the sulcal boundaries of the left medial wall in that plane. The displayed region of interest was confined to the coordinates comfortably capturing the frontal lobe. To visualise the grid contacts, the CT contour was thresholded at the Hounsfield value that optimally identified them visually, and the displayed region of interest was confined to display the stimulated grids in the target region of the medial wall. The *y* and *z* coordinates for the region of interest were plotted using ParaView's native axis display function.

## Functional imaging

*Data acquisition*

The same protocol was followed in both patients. Functional MRI data were acquired as gradient-echo planar T2*-weighted images providing blood oxygenation level–dependent (BOLD) contrast. Echo time (TE) was 30 ms and repetition time (TR) 4.5 s. Each volume

comprised 58 contiguous 2.5 mm oblique axial slices, through the temporal and frontal lobes with a 24cm field of view, 96 x 96 matrix, reconstructed to 128 x 128 for an in-plane resolution of 1.88 x 1.88mm. The field of view was positioned to maximize coverage of the frontal and temporal lobes. The data were acquired on 3T General Electric Excite HDx scanner (General Electric, Milwaukee, WI, USA). All functional imaging was done before implantation.

The task consisted of eight blocks lasting 30 seconds each, interspersed with periods of rest fixation of the same length, where the patients were visually presented with concrete nouns every 3s, and were asked either covertly to generate verbs associated with these nouns (indicated by the letter ''G'' preceding the noun), or silently to repeat the nouns presented (indicated by the letter ''R'' preceding the noun). Each block contained trials of the same type, with the verb generation and noun repetition alternating across blocks.

*Analysis*

Imaging data were analysed using SPM12 (http://www.fil.ion.ucl.ac.uk/spm/). The imaging time-series of each subject was realigned using the mean image as a reference, and smoothed with a Gaussian kernel of 8 mm full-width half maximum (FWHM). At each voxel, the time-series BOLD data were entered into a general linear model with the conditions modelled as a box-car function regressors convolved with a standard haemodynamic response function. The realignment parameters were added as nuisance regressors to minimize artefactual activation owing to head movement correlated with the task. The main effect of task was estimated separately for each condition. The SPM($t$) images were thresholded at $p$<0.05 FWE corrected, except in the noun repetition condition for DH were the level of activation necessitated the lower threshold of $p$<0.001. So as to bring the statistical maps into MNI space, the mean image was rigidly co-registered to the preimplantation structural MR volume, and the deformation field from the structural MR normalisation described in the preceding section was applied to each SPM($t$) map.

*Visualisation*

So as to visualise the areas of significant activation on the medial wall, the normalised SPM($t$) maps were rendered in ParaView (http://www.paraview.org/) as thresholded 3D contours, with the thresholds set as described above. The displayed region of interest was confined to the medial frontal wall, extending into the left hemisphere as far as x = -4 and into the right as far as its medial surface. Noun repetition and verb generation are expected to differ in the relative balance of supplementary motor area and presupplementary motor area involvement: rather than show the explicit contrast between them here we plotted both in different colours, semi-transparently rendered so as to display their overlap.

## Electrode grid implantation and stimulation

A standard clinical approach was adopted in each patient. In brief, the previously described structural MR imaging was used to plan the implantation of subdural grid and strip

electrodes (AD-TECH R Medical Instrument Corporation), which was performed through a frontoparietal craniotomy. In both patients, high-density electrode grids (5mm centre-to-centre inter-contact spacing) were used for left mesial frontal cortex coverage, whilst larger 8x8 grids (10mm centre-to-centre inter-contact spacing) and electrode strips were used to cover other regions (see Figure S3 and Table S2). Electrode localisation was confirmed via intra-operative photographs, and by post-operative CT as described above.

Post-operative cortical stimulation was performed using bipolar stimulation techniques[S3]. To avoid stimulation induced seizures, antiepileptic medication was reintroduced prior to cortical stimulation mapping (see Table S1). Trains of 50-Hz, bi-phasic square wave pulses of an AC-current with a pulse width of 500microseconds were delivered by a Nicolet™ cortical stimulator used with C64-OR amplifiers and a Nicolet Cortical stimulator Control unit (ISO 13485, ISO 9001; Nicolet Biomedical, Madison, US). Current intensity was gradually increased from 1mA in increments of 0.5 or 1mA up to 7.5mA (15 mA peak to peak of the biphasic stimulus), until the occurrence of a clinically obvious change or after-discharges on EEG monitoring. The interval between increments varied depending on the presence or absence of either behavioural or neurophysiological manifestations but was generally no shorter than 30 seconds. In line with clinical practice, so as to detect any task-invariant behavioural effects, stimulation was initially performed at rest: where incrementing to 3 to 4 mA could be achieved without visible or patient-reported motor or sensory phenomena, task-specific performance was subsequently evaluated. This clinical requirement inevitably constrained the number of sites where task-specific effects could be explored: only where no overt behaviour is triggered by stimulation can the effect on a task be fruitfully examined.

The stimulation currents for the specific tasks and electrodes reported here are presented in Table S2. Intracranial EEG data were simultaneously recorded throughout stimulation on a 128-channel NicoletOne™ LTM system (Nicolet Biomedical, Madison, US) sampling at 512 Hz.

## Behavioural tasks

*Data acquisition*

The behavioural evaluation followed standard clinical practice, which is deliberately flexible so as to adapt to the patient's specific requirements and abilities. All testing was carried out in the patient's telemetry room, during continuous video, audio, and neurophysiological monitoring, with two neurological clinicians and a neurophysiologist present. As outlined above, stimulation began at low currents, with the patient at rest, escalation both to higher currents and during behavioural tasks only where the absence of overt behavioural effects—either reported by the patient or observed by the clinician—made this possible.

The manual task consisted of rhythmic flexion-extension movements at the metacarpophalangeal joints of each hand, either unilaterally or both hands together, and

either one finger or all at the same time. The vocal task consisted of repeated utterance of a single syllable such as "la", "ma", or "ta", or reading aloud of a fixed paragraph of text. For each task, the desired movement was first demonstrated to the patient, then he or she performed it unprompted. Although a rate of two or three Hz was implicitly suggested in the demonstration, the patient was free to choose whatever rate felt most comfortable, but was encouraged to keep it constant. No temporal entraining of any kind was applied. The patient was instructed to continue the behaviour until either a request from the clinician to stop or a perceived physical change of any kind: sensory, motor, or cognitive. Stimulation was applied during this interval, at a manually randomised onset in relation to the beginning of the behaviour, and continued for a few seconds or until a behavioural change was observed or reported by the patient. Although the patient naturally knew a stimulation would be performed at some point during the action, no warning of the specific point of onset was given. Where no behavioural effect was observed, the stimulation intensity was escalated as described above until either a response was elicited or the maximum threshold was reached. Where the effect was equivocal, clinically, the stimulation was repeated once with the same parameters. The same behavioural tasks were as far as possible tested for each adjacent pair of electrode locations. The presence of after-discharges limited testing at a small minority of sites; no after-discharges were seen at our critical sites.

In our two patients, during stimulation at the critical electrodes, the manual task performed by DH was bimanual, and involved all fingers; in LW it was unimanual and involved the index finger. The vocal task in DH involved the syllable 'ta'; in LW the syllable 'la'. The video and/or audio record for both tasks when the critical electrodes were stimulated is available in the supplemental video material. Table S2 provides a summary of the behavioural parameters together with details of the post-hoc statistical tests based on the mixed general linear model quoted in the main text.

The accelerated manual behaviour seen in DH and vocal behaviour seen in LW was captured after stimulation of a unique electrode pair in each case. To investigate the anatomical specificity of the effects, we also present in Table S2 the results of stimulation at neighbouring electrodes, obtained across a range of tasks.

Note that cortical stimulation is carried out for clinical purposes, within a highly individualised context that introduces inevitable variations between patients, in addition to those resulting from different electrode placement. Crucially, the ability to perform a task during stimulation was conditional on there being no overt behavioural response that would otherwise interfere with performance. This included both motor and sensory phenomena. After-discharges and overt epileptiform neurophysiological phenomena also limited testing at some sites.

The relatively rostral localisation of the majority of DH's electrode contacts—where overt behavioural effects are rarely observed—explains the large proportion of sites open to investigation of task performance. Where enough data was available to allow a quantitative assessment (a *t*-test comparing pre- and post-stimulation rate; see Supplemental Methods),

no significant effects were found (see Table S2). Other stimulation effects in the non-critical electrodes—such as sensory phenomena—were largely restricted to electrodes located on the posterior edge of the grid. Note that conditions where there were too few syllables or taps (<4) were not quantitatively analysed. In this *post hoc* analysis, all *p* values are greater than 0.05 uncorrected (shown), and therefore further Bonferroni adjustment will not affect the inference.

The scope of task-related stimulation trials was limited in LW by overt sensory and movement phenomena that precluded the performance of any task (see Table S2).

*Data analysis: movement parameterisation*

The patient's motor behaviour was parameterised and quantified from the telemetry video and audio data using custom scripts written in Matlab (The MathWorks, Inc., Natick, MA). In brief, the timing of each finger movement was determined by extracting a time-series of greyscale image intensity values (at the original video sample rate of 25 frames per second) within a manually defined region-of-interest enclosing the fingers. This produced an oscillating trace where the peaks corresponded to each cycle of movement; this was manually checked in each case (Figure S1). For the purposes of detecting a stimulation-induced change, the frequency of alternation was then calculated as the reciprocal of the mean time delay between the neighbouring (preceding two) movements. For the reciprobit analysis (see below) each inter-movement interval was analysed independently.

Vocal data were extracted from the audio channel of the video telemetry record (16 bit, sampled at 11kHz) and high pass filtered at 300Hz using a Finite Impulse Response filter implemented in Fieldtrip (http://www.ru.nl/neuroimaging/fieldtrip/)[S4] to remove background noise. The upper Root Mean Square envelope of this signal provided a 'volume envelope' time-series of speech, each peak identifying a syllable. Matlab's peak detection algorithm was then used to determine the timing of spoken syllables from this signal (Supplemental Figure S2). As in the manual task, the parameterisation was verified by inspection, and non-speech sounds (such as breaths) removed before conversion to behavioural frequency as above.

*Data analysis: inference*

The behavioural effect of stimulation at the critical locus was clinically apparent. To formalise the inference, we entered baseline and stimulation frequency values into a mixed general linear model, with subject as a random factor and effector modality (vocal versus manual) and stimulation (pre or post) as fixed factors. Post hoc *t*-tests were used to interrogate significant effects. To account for multiple comparisons, we performed a Bonferroni adjustment to the critical threshold of alpha=0.05.

The baseline and stimulation periods included in the models were defined separately for each condition and designed to be cognizant of the effector-specific effects of stimulation, controlling for as many parameters as is possible in this clinical scenario, where stimulation

lengths and block lengths varied. Note that since the timing of the clinical manifestations relative to the onset and offset of stimulation is substantially variable, and differs across effectors—generally showing greater latency for speech than for manual movements[S5]—there is neither a hard criterion for setting the correct lag nor plausible grounds for keeping it the same across effectors. In keeping with the clinically observed effector-specific differences, for the manual task we therefore set the lag relatively short, at 200ms, comparing a 4 second baseline window to a stimulation window beginning 200ms after the onset of stimulation and extending for a further 1.2 seconds beyond the offset of stimulation. For the vocal task, where a slower onset is to be expected, the stimulation window was set 2 seconds after the onset of the stimulation, continuing for 2 seconds after offset. The correspondence with the data is illustrated by a first order spline, fit using a robust minimisation of ordinary least squares with breakpoints at the baseline and stimulation window edges (implemented in the SplineFit Toolbox http://uk.mathworks.com/matlabcentral/fileexchange/13812-splinefit) and shown in the bottom panels of Figures S1 & S2.

Where the vocal task consisted of reading, the syllable separation is naturally reliant on the sensitivity of the volume envelope to neighbouring phonemic differences, which are also likely to be less pronounced within words than between them. This effect can be viewed as modest downsampling of the data (because some syllables will be missed). It cannot plausibly create spurious components, nor plausibly interact with stimulation in a way that may confound the result.

To make our analysis sufficiently robust, we rejected behavioural trials where the total number of syllables or finger movements recorded was too low for a statistical analysis to be meaningful (n<4), in either the pre or post-stimulation conditions.

*LATER modelling*

To explore the correspondence of the data to a LATER model of action here, we transformed the inter-movement intervals, for each of the two conditions where a significant stimulation effect was observed, into their reciprocals and plotted them against their $z$-scores, assuming them to be Gaussian in their distribution after the transformation. An overview of the underlying LATER model is given in Figure 1, and of such "reciprobit" plots in Figure 3 of the main text.

The data from each condition were separately fitted to the output of LATER models of the early (where present) and main components of the transformed distributions. In the pre-stimulation data—defining the default behaviour—the main component was modelled as a ramp process racing at rate $r$ to a threshold of fixed height $\theta=1$ above baseline. Three parameters are allowed to vary: $\mu$, $\sigma_1$, and $\sigma_2$. The rate of rise, $r$, is a random Gaussian variable of mean, $\mu$, and standard deviation, $\sigma_1$. The early component process rises at a rate set at '0', with much larger standard deviation, $\sigma_2$. To determine the effect of stimulation, four different models of the post-stimulation data were separately fitted for each condition (manual and vocal), where the three standard parameters were constrained to different extents. The "Null" model assumes no effect of stimulation, and fits both pre- and post-

stimulation data with the same parameters. The "Unconstrained" model, treats the pre- and post-stimulation data as unrelated, allowing all three parameters to vary freely. The "Swivel" model is identical to the "Null" model except that the $\theta$ parameter is no longer fixed at 1, and is allowed to change with stimulation. The "Shift" model is identical to the "Null" model except that the $\mu$ parameter is allowed to change with stimulation.

These models correspond to materially different physiological effects of stimulation on the underlying behaviour, as conceptualised within LATER. A "Swivel", where stimulation produces a rotation of the modelled distribution around an intercept at infinity, implies a change in the threshold that a process must reach first to become manifest in behaviour. A "Shift", where stimulation produces a horizontal displacement of the modelled distribution along the abscissa, implies a change in the rate of rise of the competing processes. The other two—"Null" and "Unconstrained"—model either the absence of any stimulation effect, or its indifference to the distinction that shift and swivel define.

All models were estimated by minimising their negative log likelihood, which was then summed across subjects to provide a cumulative log likelihood per model. To compare the models, we used the Bayesian Information Criterion (BIC), which optimally balances differences in log likelihood taking into consideration model complexity (the number of model parameters that can vary) and number of data samples. We also supply a categorial interpretation of the strength of the evidence provided, based on BIC and its relation to the Bayes Factor (e.g. change in BIC >~2.2 is substantial positive evidence, change in BIC>~6 is very strong evidence) [S6]. The comparison of models allows inferences to be made on whether the effect of stimulation is most parsimoniously explained by a change in distance to threshold, $\theta$ ('Swivel'), mean rate of rise $\mu$ ('Shift'), or neither alone ('Unconstrained'), as compared to the 'Null' model.

In a further, corroborative analysis, we extracted the maximum likelihood value of the parameters of interest from the winning model, and calculated their confidence intervals with the aid of a bootstrap procedure. Data from the pre- and post-stimulation conditions (separately for manual and vocal responses) were randomly resampled with replacement to create an artificial dataset of the same size as the original, from which the model could be repeatedly re-estimated. This procedure was performed 1000 times and the 2.5% and 97.5% centiles of the resulting parameter estimates were used to approximate the 95% confidence intervals[S7].

These analyses were performed with the aid of Mike Shadlen's Reciprobit Toolbox v1.0 for Matlab (https://www.shadlenlab.columbia.edu/), in addition to custom Matlab scripts available from the authors.

## Supplemental References


S1. Manjón, J.V., Coupé, P., Buades, A., Louis Collins, D., and Robles, M. (2012). New methods for MRI denoising based on sparseness and self-similarity. Medical Image Analysis *16*, 18–27.

S2. Grachev, I.D., Berdichevsky, D., Rauch, S.L., Heckers, S., Kennedy, D.N., Caviness, V.S., and Alpert, N.M. (1999). A method for assessing the accuracy of intersubject registration of the human brain using anatomic landmarks. Neuroimage *9*, 250–268.

S3. Kovac, S., Scott, C.A., Maglajlija, V., Toms, N., Rodionov, R., Miserocchi, A., McEvoy, A.W., and Diehl, B. (2014). Comparison of bipolar versus monopolar extraoperative electrical cortical stimulation mapping in patients with focal epilepsy. Clinical Neurophysiology *125*, 667–674.

S4. Oostenveld, R., Fries, P., Maris, E., and Schoffelen, J.-M. (2010). FieldTrip: Open Source Software for Advanced Analysis of MEG, EEG, and Invasive Electrophysiological Data. Computational Intelligence and Neuroscience *2011*, e156869.

S5. Kovac, S., Scott, C.A., Maglajlija, V., Rodionov, R., McEvoy, A.W., and Diehl, B. (2011). Extraoperative Electrical Cortical Stimulation: Characteristics of Motor Responses and Correlation with Precentral Gyrus. Journal of Clinical Neurophysiology *28*, 618–624.

S6. Kass, R.E., and Raftery, A.E. (1995). Bayes Factors. Journal of the American Statistical Association *90*, 773–795.

S7. Efron, B., and Tibshirani, R. (1986). Bootstrap Methods for Standard Errors, Confidence Intervals, and Other Measures of Statistical Accuracy. Statist. Sci. *1*, 54–75.